



Viscous fingering instability in one-end-lifted Hele-Shaw cells for producing three-dimensional hierarchical structures

Wenchang Zhao^a, Shiyu Wang^a, Ying Zhou^a, Min Wang^a, Ling Yang^b, Jun Liu^c, Liqiu Wang^d, Pingan Zhu^{a,e,*}

^a Department of Mechanical Engineering, City University of Hong Kong, Hong Kong, China

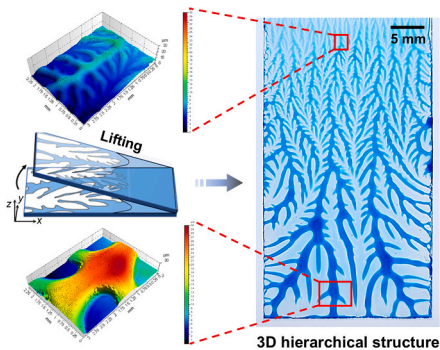
^b Department of Mechanical Engineering, The University of Hong Kong, Hong Kong, China

^c Department of Data and Systems Engineering, The University of Hong Kong, Hong Kong, China

^d Department of Mechanical Engineering, The Hong Kong Polytechnic University, Hong Kong, China

^e Shenzhen Research Institute of City University of Hong Kong, Shenzhen, China

GRAPHICAL ABSTRACT



ARTICLE INFO

Keywords:

Leverage fingering instability
One-end-lifted HSCs
Varying boundaries
Hierarchical structures
Nonclonable
Anti-counterfeiting

ABSTRACT

Hypothesis: The focal research on viscous fingering (VF) instabilities has primarily concentrated on alleviating and suppressing this phenomenon, but the potential to enhance and leverage them for developing practical applications remains inadequately explored. VF occurs when a less viscous fluid displaces a higher viscous fluid, governed by fluid dynamics and resulting in finger-like patterns at their interface in a facile and gentle way, yet sensitive to initial and boundary conditions, such as fluid type and cell thickness, giving rise to many bifurcating structures.

Experiments: Leveraging Hele-Shaw cells (HSCs) with changing thicknesses that induced varying boundary conditions, we systematically investigated the characteristics of VF under these conditions and developed applications based on our findings.

Findings: We introduce VF in one-end-lifted HSCs to enhance VF rather than suppression to achieve satisfactory tunability of finger size and harness it to explore application. It enables the moldless, facile, scalable, and cost-effective fabrication of diverse hierarchical structures derived from branched patterns composed of numerous dense fingers with progressively decreasing sizes. With this phenomenon, the finger width scales inversely with

* Corresponding author at: Department of Mechanical Engineering, City University of Hong Kong, Hong Kong, China.

E-mail address: pingazhu@cityu.edu.hk (P. Zhu).

<https://doi.org/10.1016/j.jcis.2025.138202>

Received 4 February 2025; Received in revised form 12 June 2025; Accepted 14 June 2025

Available online 17 June 2025

0021-9797/© 2025 Published by Elsevier Inc.

the capillary number raised to the power in a range between -0.53 to -1.22 , depending on the varying boundary conditions. By capitalizing on the hierarchy and specific distribution ridge of the fingering patterns, the fabricated fractal structures exhibit physically nonclonable characteristics, offering promising applications in anti-counterfeiting.

1. Introduction

Viscous fingering (VF) instability serves as an archetype in various processes, including printing [1], fluid mixing [2], chromatographic separation [3], CO₂ sequestration [4], and granular flow [5]. VF is characterized by the formation of finger-like patterns when a low-viscosity fluid invades a high-viscosity fluid, where the two fluids can be either immiscible [2,6,7] or miscible [8–11]. Since the seminal work by Saffman and Taylor in 1958 [6], significant advancements have been made in understanding VF [12–14]. In the case of fluid displacement in two immiscible fluids, the narrowing of the finger is driven by viscous forces, while the blunting of the finger is caused by interfacial tension forces. Consequently, infinitesimal perturbations with long wavelengths grow, while those with short wavelengths are suppressed by interfacial tension. The width of the fingers is decided by the critical wavelength of the instability (λ_c), which scales with the capillary number (Ca , the ratio of viscous to interfacial tension forces) as $Ca^{-1/2}$, beyond which the finger bifurcates. On the other hand, fractal fingers emerge in scenarios involving fluid displacement in porous media [11], miscible fluids with one phase being a non-Newtonian fluid [15], and granular systems in the zero-surface-tension limit [5].

VF is sensitive to initial and boundary conditions. Seemingly insignificant perturbations can have a pronounced impact on instability, leading to variations and diversities in the shapes and characteristics of VF. Extensive efforts have been devoted to controlling fingering patterns through engineering the setup, a two-dimensional Hele-Shaw cell (HSC) consisting of two plates separated by a thin fluid gap, with examples including entraining a bubble [16], embedding wires [17], and structuring plates [18]. Inspired by the time-dependent channel geometry found in practical applications like respiratory airflows in lungs [19], liquid transfer in printing processes [20], and separation between two bodies connected by a thin adhesive layer [21], dynamic HSCs with rotated [22] and lifted [23–26] plates have been proposed to tailor VF. It is important to note that VF is generally considered to be detrimental because it hinders the operation of the processes and limits their efficiency, such as limiting the recovery rate in the oil industry and reducing printing uniformity. Therefore, the suppression of VF has been a focal point in recent studies and can be achieved through various means such as variational injection rates [27,28], elastic membranes [29,30], tapered flow geometries [31–33], time-dependent gap thickness [34], surface wettability modifications [35], porous media with a pore size gradient [36], and active control of electro-osmotic flows [37]. Despite these accomplishments, the enhancement rather than suppression of VF to exert its advantages has yet to be fully demonstrated, leading to broad appeal for the development of suitable applications leveraging VF.

Once viewed as a concern, VF is now increasingly harnessed to develop practical applications. By forming finger-like structures, VF can increase the contact area between fluids, thereby shortening diffusion paths to enhance mixing efficiency. This property enables efficient mixing of multi-component fluids in microfluidic channels and micromixers, which is favorable for chemical and biological reactions [2,38]. Moreover, the highly branched nature of finger-like structures facilitates the development of biomimetic structures, such as replicating dendritic vascular networks [39] and preparing hydrogel lumens for tissue model simulations [40], holding promise for tissue engineering and regenerative medicine. Additionally, the branched structures formed by VFs can increase the effective area for fluid dispersion; compared to uniform discs, a smaller volume of fluid can cover a larger surface area in a branched configuration, allowing for rapid material spreading [41].

Although the harness of VF has been proven in the fields mentioned above, the finger-like structures used often exhibit poor size tunability, limiting the application scope. This limitation arises from the VF operating under fixed boundary conditions, constrained by factors such as the size of HSCs, gap thickness, and low Ca values, making it challenging to generate small fingers and resulting in a narrow size adjustment range. If size-tunable finger-like structures can be developed within a single cell, this capability could facilitate new applications, such as the preparation of hierarchical structures. Hierarchical structures are composed of multiple interrelated levels across various scales or functions. It is prevalent in both nature and engineering, enhancing the performance and functionality of materials [42]. Fabrication methods such as embossing [43,44], microimprint [45,46], Inkjet printing [47], soft lithography [48,49], 3D printing [50,51], and laser scanning [52,53] have made significant progress in fabricating hierarchical structures. However, these techniques require expensive, sophisticated instruments and involve cumbersome procedures, making them time-consuming and prone to errors. Additionally, the necessity of custom molds in most processes further complicates and increases costs. Therefore, there is an urgent need for a cost-effective and straightforward preparation method. As a prototype for pattern formation, VF can generate highly branched structures in a mold-free and facile manner, but whether satisfactory tunability of finger size can be realized in a single device to achieve hierarchy remains questionable.

In this study, we utilized VF in one-end-lifted HSCs with dynamically changing cell thickness to achieve adequate tunability of finger size for the preparation of hierarchical structures. Through this approach, fingers bifurcate continuously with diminishing widths, resulting in hierarchical patterns. Simultaneously, the inherent heterogeneity, irregularities, and fluctuations within the system contribute to the variability in the details of the fingering patterns, including specific shapes and branching structures. We observe that the finger width scales inversely to Ca with a power in a range between -0.53 to -1.22 , in contrast to the classical scaling of $\sim Ca^{-1/2}$ [12–14], demonstrating the significant dependence of VF on varying boundary conditions. Leveraging the above-mentioned VF, we demonstrate the moldless fabrication of hierarchical structures with high complexity in fractal structures and rich diversity in fingering patterns. These findings highlight physical nonclonability and hold significant promise for anti-counterfeit applications.

2. Experimental section

2.1. Experimental conditions

The one-end-lifted HSC employed in our experiments consists of two substrates made of glass, except for those engineered substrates with predetermined patterns, where acrylic was used. Prior to the experiments, the two substrates are aligned in parallel and secured together at one end using tape. The surface area available for the high-viscosity liquid within the HSC can be adjusted flexibly by modifying the size of the overlapping region between the two substrates.

For the investigation of fingering instability dynamics, we employed an air-silicone oil (Macklin) system. Silicone oils with different viscosities (200, 500, 750, and 1000 mPa s) were used as the high-viscosity liquid. In the fabrication of solid structures, we utilized a polystyrene (Aladdin) solution dissolved in toluene (Anaque) and hot molten paraffin (Aladdin) as the high-viscosity liquids, with air serving as the low-viscosity fluid.

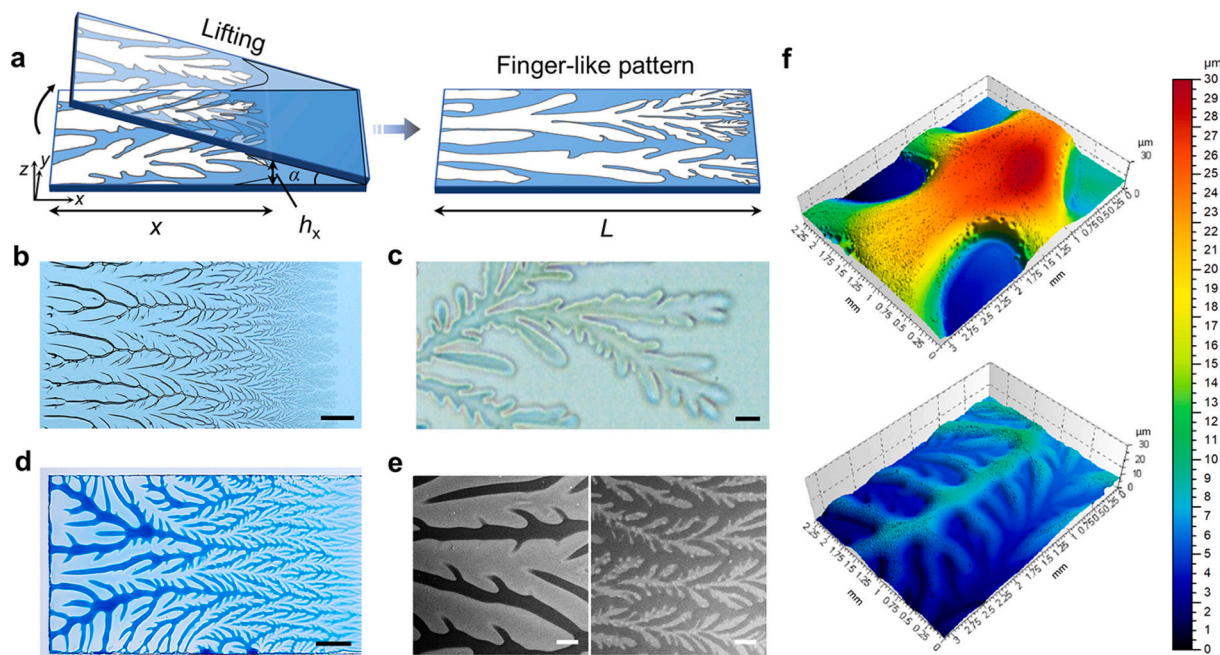


Fig. 1. Viscous fingering instability in a one-end-lifted Hele-Shaw cell. a) Schematic of the experimental setup of the one-end-lifted (z -axis direction) Hele-Shaw cell to produce hierarchical patterns. b) A snapshot capturing the formation of a hierarchical finger-like pattern as air displaces silicone oil (500 mPa s). c) The smallest finger size observed under an optical microscope. d) The formed polystyrene hierarchical structure with the evaporation of toluene. e) Scanning electronic microscopy images and f) optical surface profiler images of two representative regions of a polystyrene pattern exhibiting hierarchy in both the width and height of the structure. In e), the dark black area represents the polystyrene structure. Scale bars are 3 mm in b), 20 μm in c), 5 mm in d), and 1 mm in e).

To control the lifting of the free end of the lifted substrate, we employed a syringe pump (Syringe Pump LSP01-1A) that maintained a constant lifting speed (Fig. S1). In our experiments, three different lifting speeds were utilized: 0.32, 0.48, and 0.80 mm/s, corresponding to the experimental groups Exp1, Exp2, and Exp3, respectively. As the HSC is placed horizontally and the liquid film thickness is extremely thin, approximately 10 μm , the effect of gravity can be considered negligible.

2.2. Fingering instability experiments

To induce fingering instability, the device was placed horizontally, with the bottom substrate fixed, while the upper substrate was capable of lifting around the fixed end in a direction perpendicular to the bottom substrate. To establish the liquid film within the HSC, a known mass (m) of liquid (density ρ) was initially deposited on the bottom substrate. Subsequently, the upper substrate is pressed onto the liquid droplet, ensuring that the entire overlapping region with an area of S is filled. After a waiting period of approximately 30 s, the liquid film stabilizes with a predetermined thickness of $h_0 = m / \rho S$. By lifting the upper substrate, air from the surrounding environment infiltrates the liquid film, resulting in the formation of finger-like patterns.

The process of pattern formation was recorded using a high-speed camera (Fastcam Mini, Photron) at a frame rate of up to 4000 frames per second. The recorded videos and images were subsequently analyzed utilizing the open-source software ImageJ (National Institutes of Health) for further investigation and data extraction.

3. Results

3.1. Viscous fingering instability in a one-end-lifted Hele-Shaw cell

The one-end-lifted HSC, as illustrated in Fig. 1a, comprises a stationary substrate and a lifted substrate propelled by a pump at a constant speed (Fig. S1). Initially, the two substrates are parallel to each other, with an intersected angle α of zero. A predetermined mass of high-

viscosity liquid (typically silicone oil, unless otherwise specified) is confined between the two parallel substrates, resulting in a thin liquid film with an initial thickness of h_0 (around 10 μm). As the substrate lifts, low-viscosity air infiltrates the liquid film, creating a progressing interface where VF takes place, giving rise to finger-like patterns. The experimental region's length is denoted as L , while x represents the real-time position of the interface, and h_x corresponds to the liquid film thickness at position x . Fig. 1b showcases the VF characterized by densely protruding fingers that decrease in width from left to right (Video S1). The dimensions of the viscous fingers can vary significantly, ranging from several millimeters (Fig. 1b) to around ten micrometers (Fig. 1c and Video S2) determined by the film thickness h_0 , spanning two orders of magnitude.

To translate the VF patterns into tangible hierarchical structures, we employ a solution of polystyrene dissolved in toluene (25 wt%) serving as the high-viscosity liquid (580 mPa s). After the evaporation of toluene, the VF pattern solidifies (Fig. 1d). The cured pattern can maintain its integrity even after half a year (Fig. S2). Scanning electron microscope (SEM) images vividly demonstrate the contrasting widths of the fingers in different regions (Fig. 1e). Furthermore, three-dimensional (3D) optical profilometer results reveal variations in the height of the polystyrene structure (Fig. 1f). Furthermore, lower polystyrene content results in reduced solution viscosity, corresponding to a decreased structure height. As shown in Fig. S3, hierarchical structures were prepared using polystyrene solutions with varying concentrations (15 wt%, 20 wt%, and 25 wt%). The results indicate that structural height increases with the viscosity of the solution under the same conditions. Consequently, the proposed strategy enables the one-step, moldless fabrication of intricate 3D hierarchical structures.

3.2. Dynamics of viscous fingering instability in a one-end-lifted Hele-Shaw cell

Fig. 2a illustrates the temporal evolution of VF in one-end-lifted HSCs. As air protrudes into the liquid, finger-like structures

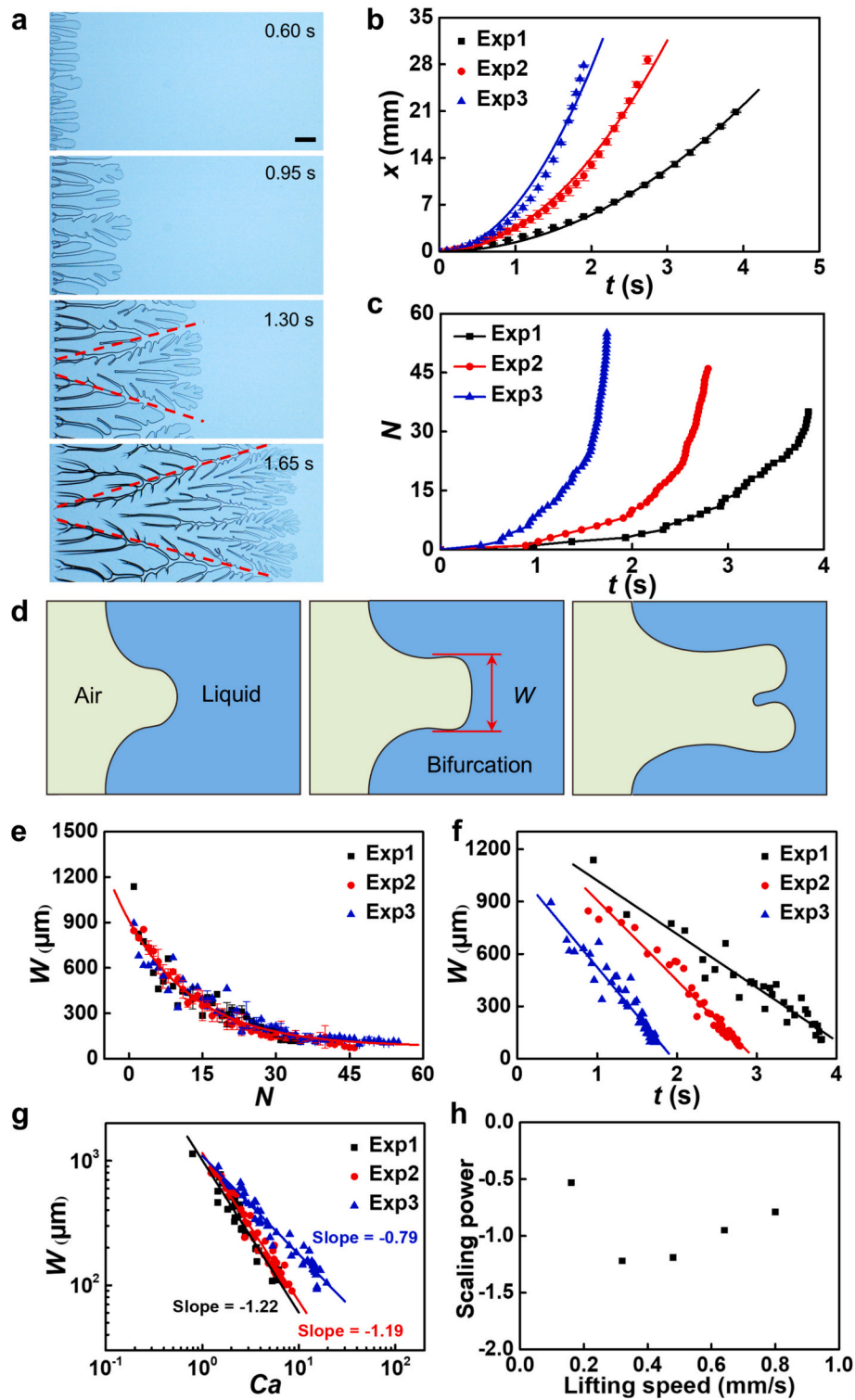


Fig. 2. Dynamics of viscous fingering instability in a one-end-lifted Hele-Shaw cell. a) Temporal evolution of the finger-like pattern in an air-silicon oil system. The red dotted lines indicate the boundaries of the dominant finger, illustrating the coexistence of longitudinal spreading and transverse expansion of the fingers. Scale bar, 2 mm. b) The plot of the real-time location (x) of the liquid film against time (t). The solid lines represent quadratic-function fittings to the data. c) The plot of the number of bifurcations (N) as a function of time (t), demonstrating an accelerated bifurcation of fingertips. d) A schematic depicting the characteristic finger width (W) defined at the instant of bifurcation. e) The relationship between W and N , with a red line indicating an exponential fit to the data. f) The decrease of W with t is an almost linear manner. The fitting slopes are $-306 \mu\text{m/s}$, $-458 \mu\text{m/s}$, and $-550 \mu\text{m/s}$ for experimental groups Exp1, Exp2, and Exp3, respectively. g) The scaling law between the finger width (W) and capillary number (Ca). h) The plot of scaling power versus lifting speed. (For interpretation of the references to colour in this figure legend, the reader is referred to the web version of this article.)

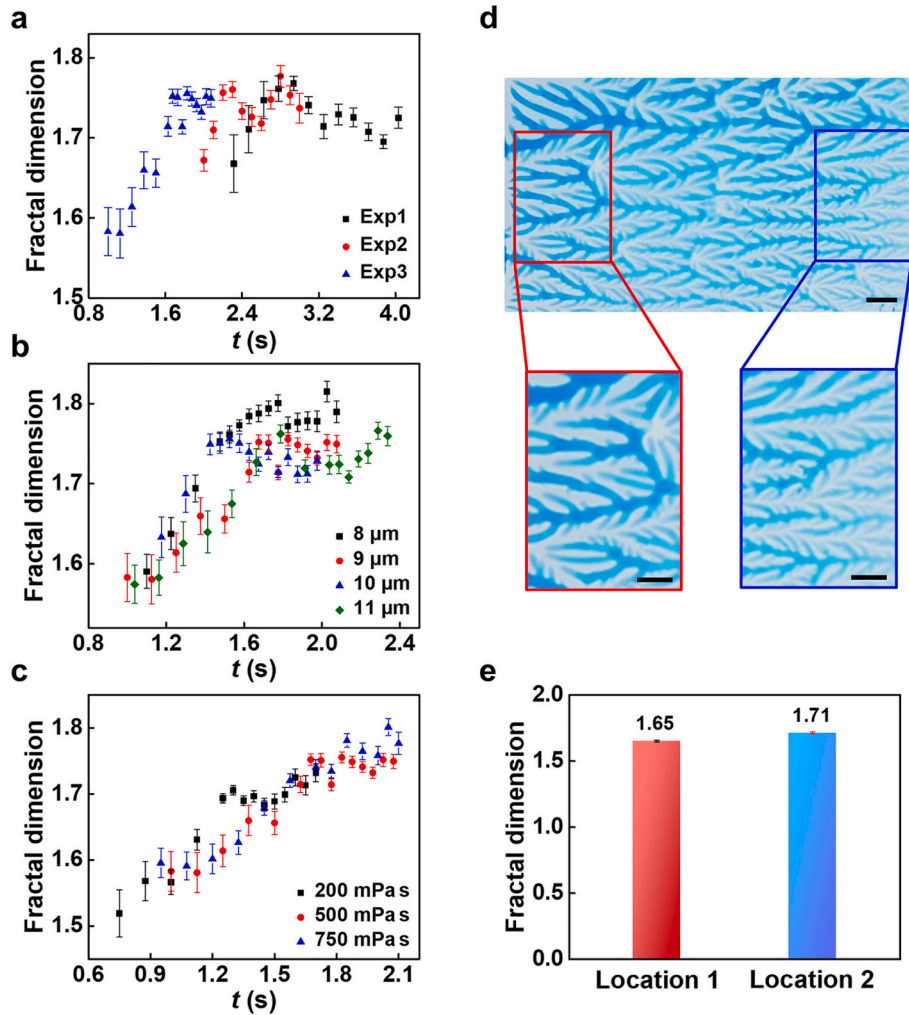


Fig. 3. Fractal dimension. a-c) The plot of the fractal dimension (d_f) of the pattern against time (t) in an air-silicon oil system, considering different lifting speeds, initial film thicknesses, and liquid viscosities. d) A comparison of the fractal structures in two regions of the produced solid hierarchical pattern. Scale bar, 3 mm. e) The fractal dimension of the two regions shown in d).

continuously evolve, exhibiting a multitude of fingertip bifurcations. During this development, the fingers grow through both transversal expansion and longitudinal spreading (Fig. 2a, 1.3 s). An intriguing shielding effect becomes apparent among the fingers: when one finger advances, it eventually dominates over its neighbors, inhibiting their growth (Fig. 2a, 1.3 s and 1.65 s). The resulting fingering pattern is characterized by a highly ramified morphology, with a gradient of decreasing finger sizes.

To examine the pattern growth, we conducted three sets of experiments involving different lifting speeds at one end of the lifted plate (0.32 mm/s, 0.48 mm/s, and 0.80 mm/s in Exp1, Exp2, and Exp3, respectively, see Fig. S4). Fig. 2b illustrates the temporal progression of the longitudinal spreading position of the fingers, demonstrating a quadratic growth over time until the final stages of pattern development. Consequently, the velocity at which a single finger advances, denoted as U , exhibits an almost linear increase with time, characterized by two distinct stages (Fig. S5). It is important to note that the second stage occurs within a brief timeframe and involves rapid spreading of the fingers with a diverging velocity, U . Therefore, we focus our investigation on the initial stage characterized by a slower spreading velocity to examine finger development in this study.

Tens to hundreds of fingertip bifurcations occur during the spreading process, in stark contrast to VF instabilities in previous studies, where tip-splitting is limited to a few occurrences. Fig. 2c demonstrates the

monotonic increase in the number of bifurcations (N) with time (t) based on experimental results. The frequency of bifurcation accelerates as the fingers develop, leading to a decreasing time interval between bifurcations (t_i). Fig. S6 demonstrates that t_i decreases as the number of bifurcations (N) increases, and after approximately 27 bifurcations, it reaches a nearly constant value. Furthermore, this fixed value is observed to be smaller for higher lifting speeds.

To investigate the evolution of finger size, we define the width of fingers just before bifurcation, denoted as W , as the characteristic dimension (Fig. 2d). The finger width W monotonically decreases with the number of bifurcations N and asymptotically approaches a final constant value, as depicted in Fig. 2e. Similarly, W decreases almost linearly with t , with a faster decreasing rate observed for larger lifting speeds (Exp3 > Exp2 > Exp1, Fig. 2f). The combined observations from Figs. 2e and f confirm the hierarchical VF pattern characterized by decreased size.

Figs. 2g and S7 present the dependence of the normalized finger width W on the capillary number $Ca = 12\mu U/\gamma$, where γ and μ represent the surface tension and viscosity of the high-viscosity fluid, respectively. At a low lifting speed of 0.16 mm/s, the finger width scaling follows the form of $W \sim Ca^{-0.53}$, consistent with the well-established scaling $W \sim Ca^{-1/2}$ in previous VF studies for immiscible fluids. However, as the lifting speed increases, the power is in the range of -0.79 to -1.22 and increases with the lifting speed (Fig. 2h). Further investigation of the

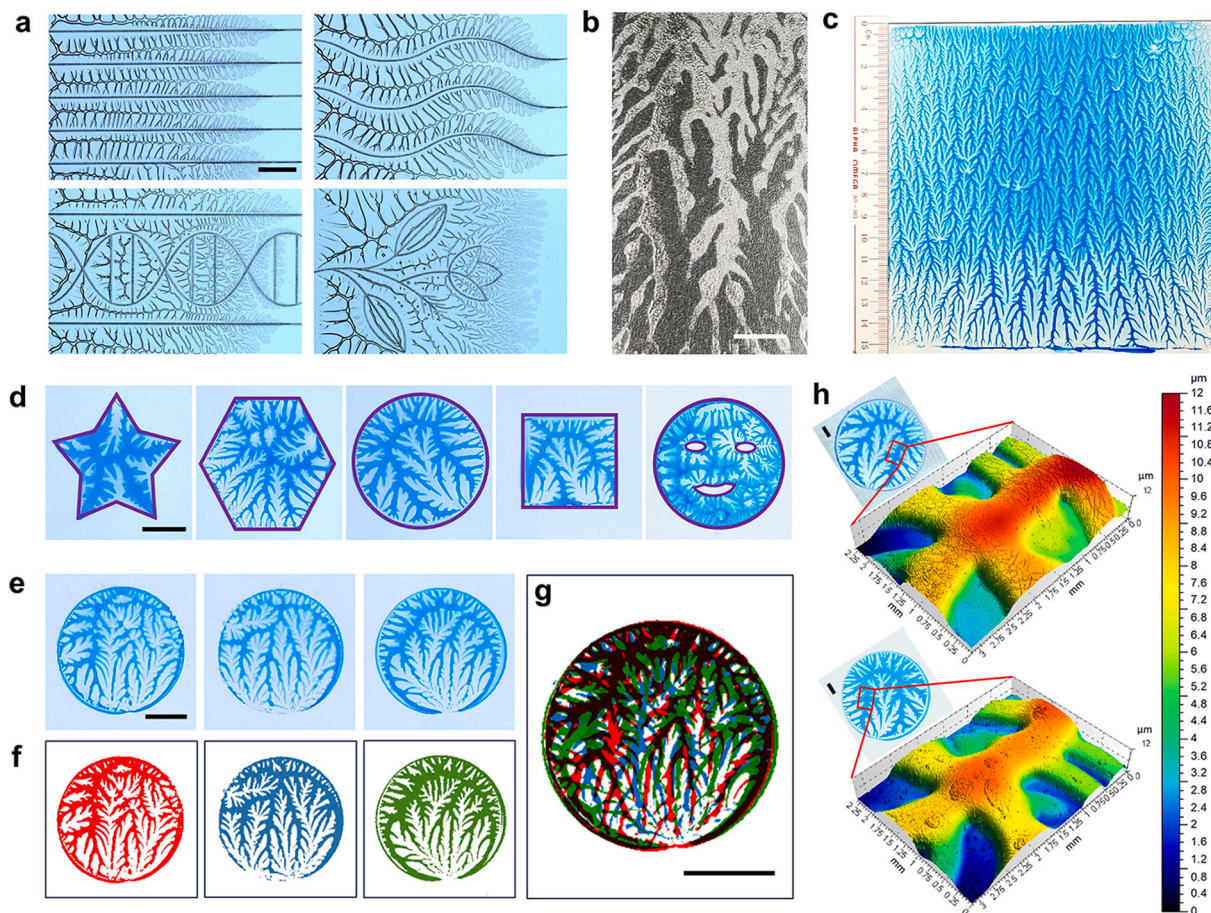


Fig. 4. Diversified hierarchical structures. a) Various hierarchical patterns achieved by engineering the substrates. b) Solid pattern created using molten paraffin as the high-viscosity liquid. c) Scaling up the production of the solid structure with a substrate size of $15 \times 15 \text{ cm}^2$. d) Customization of the exterior shape of the structures. The purple lines represent the prepared shapes, including a pentagram, hexagon, circle, square, and smiley face. e) Three solid structures fabricated under the same experimental conditions. f) Authentication information extraction for the three structures in e). g) Non-coincidence of the three patterns in f) demonstrating the distinctiveness of the structures. h) Optical surface profiler images of the same area of mirror-symmetrical polystyrene patterns formed on the lower and upper substrates simultaneously. Scale bars are 5 mm in a), b), d), e), f), and g) and 2 mm in h). (For interpretation of the references to colour in this figure legend, the reader is referred to the web version of this article.)

dependence of W on U reveals a scaling of $W \sim U^{-a}$, with the power a in a range between -0.53 and -1.22 (Fig. S8). These findings highlight the significant dependence of finger-like structures on time-varying boundary conditions resulting from the lift of the upper substrate.

3.3. Fractal dimension

To assess the overall characteristics of the fingering patterns, we employ a box-counting method to quantify their fractal dimension (d_f). This method involves covering the pattern with boxes of size l and determining the number of boxes (n) required to fully cover the pattern. The fractal dimension d_f can then be obtained as a power-law relationship, where $n \sim l^{d_f}$. For each pattern, we repeat the box-counting operation with boxes $l = 2, 3, 4, 6, 8, 12, 16, 32, 64$, separately to obtain its fractal dimension. First, the relationship between the fractal dimension and the number of bifurcations was studied. As shown in Fig. S9, d_f shows an increased trend with N , reaching a plateau around 1.65 after 40 bifurcations, indicating its self-similar growth. Figs. 3a-c illustrate the dynamic variation of d_f with time (t) under different conditions, including changes in lifting speed, initial thickness of the liquid film, and viscosity of the silicone oil. In all cases, d_f initially shows a gradual increase with time, followed by a plateau, indicating that the VF attains fully developed, self-similar properties after a certain period. It is worth noting that the final, constant d_f value falls within the range of 1.7 to 1.8,

which corresponds to the values predicted by diffusion-limited aggregation (DLA) [54,55] and invasion percolation [56] models, respectively.

Furthermore, we measure the fractal dimension of the fabricated solid hierarchical structures. A comparison is made between two representative regions, one at the beginning and the other at the end of the structure (Fig. 3d). The obtained d_f values are found to be similar in both regions, hovering around 1.68. This observation highlights the retention of self-similar properties even after the fabrication of solid structures, emphasizing the robustness of the proposed fabrication method.

3.4. Diversified hierarchical structures

The characteristics of the fabricated hierarchical structures are highly influenced by the boundary conditions of the two substrates. Carving grooves on substrates enables the creation of a diverse array of VF patterns, as depicted in Fig. 4a and Video S3. The engineered grooves are deliberately shaped as straight lines, wavy lines, double helix, flowers, and various other configurations (Fig. S10), which are designed to guide the progression of the gas-liquid interface, thereby facilitating the formation of VF structures with predetermined patterns in a simple and user-friendly manner. Importantly, even with these engineered surface patterns, the resulting structures still maintain their hierarchical

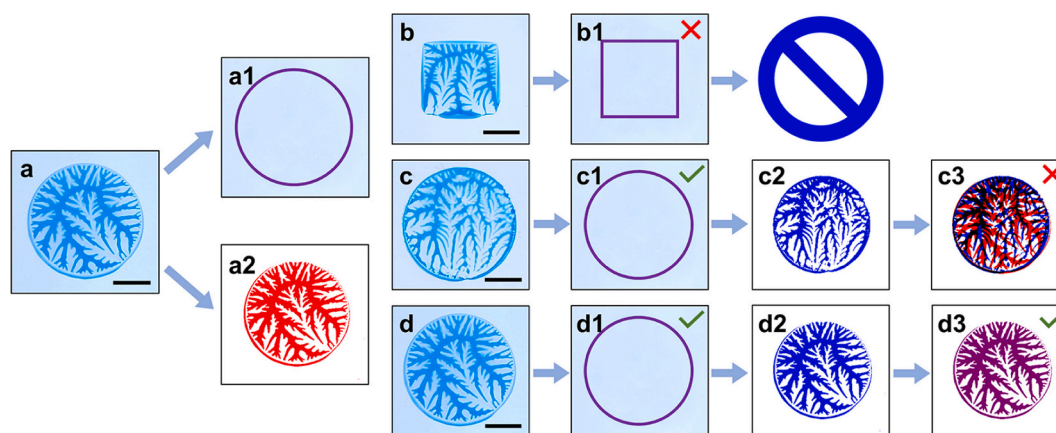


Fig. 5. Anti-counterfeiting. a-a2) Encrypted sample a) and the extracted cloneable exterior shape information a1) and uncloneable internal pattern a2). b-d) Three samples to be verified. b1-d1) Process of comparing the exterior shapes with a2). Fake samples cannot pass this verification. c2-d2) Extracted interior ridge pattern. c3-d3) Process of further verifying the interior pattern by superimposing c2) and d2) with a2). Structures with matched authentication information are marked with “√”, while those mismatching the authentication information are marked with “X”. Scale bars, 5 mm.

nature with a reduced gradient in size.

The proposed fabrication technique exhibits scalability and compatibility with various fluidizable and solidifiable materials. Fig. 4b illustrates the preparation of a solid fractal pattern using paraffin as the high-viscosity fluid. In this process, hot molten paraffin is placed between the two substrates and undergoes a phase transition from liquid to solid as the substrate is lifted, generating the VF pattern. Moreover, scalability is demonstrated in Fig. 4c, where an enlarged substrate surface area ($15 \times 15 \text{ cm}^2$) still allows the formation of hierarchical structures with noticeable dimension differences. This scalability is crucial for mass production and paves the way for practical applications. In addition, the exterior shape of the structure can be predefined using substrates with various geometries. As illustrated in Fig. S11, the shaded area of the lower substrate represents the experimental region with a specific configuration, where a high-viscosity liquid is deposited. When the upper substrate is lifted, hierarchical structures are confined in the predefined shape. Leveraging this strategy, we successfully prepared structures in the shapes of a pentagram, hexagon, circle, square, and smiley face (Fig. 4d).

Due to the susceptibility of the VF process to initial and boundary conditions, the as-prepared structures exhibit physical non-cloneability, with high complexity and rich variability. To validate this, three samples are fabricated under identical experimental conditions (Fig. 4e). The interior VF pattern ridges are extracted (Fig. 4f), and their diversities are examined by superimposing them. Fig. 4g shows that each internal pattern possesses similar hierarchical structures but distinct arrangements of ridges, displaying their non-replicability. Crucially, these structures are irreproducible even by the manufacturers. When the substrates are separated, two hierarchical structures form on the upper and lower substrates in a mirror-symmetric manner, displaying nearly identical relative distributions of ridges. However, notable differences in ridge height within the same region were still observed (Fig. 4h), further confirming their non-cloneability.

As a proof-of-concept, Fig. 5 illustrates the application of the as-prepared hierarchical structures to anti-counterfeiting purposes using a multiple encryption strategy. As shown in Figs. 5a-5a2, the encoded information involves two aspects: the cloneable exterior shape and the non-cloneable interior pattern (PUF), where the shape is encrypted to improve the verification speed. For decoding, authentication is successful only when both the exterior shape and interior pattern meet predefined criteria. For the three samples displayed in Figs. 5b-5d, the exterior shapes (Figs. 5b1-5d1) are initially extracted as the first layer of authentication information and compared with Fig. 5a1, allowing for the rapid exclusion of mismatched sample b. Subsequently, the ridges of the internal pattern from the shape-matching samples (Figs. 5c2 and

5d2) are extracted as the second layer of authentication information and superimposed with Fig. 5a2 for comparison (Figs. 5c3 and 5d3). Finally, it is concluded that sample d is the authorized sample.

4. Conclusions

We have demonstrated the formation of fingering instability in one-end-lifted HSCs, which undergoes dynamic evolution. This identified fingering instability is characterized by numerous fingertip bifurcations leading to decreasing finger widths. As a result, the resulting fingering patterns exhibit highly branched structures with hierarchical features. Utilizing various boundary conditions, we demonstrate the fabrication of hierarchical structures with high complexity in fractal structures and rich diversity in fingering patterns, confirming the utilization of VF instead of suppression. This method is mold-free, facile, scalable, cost-effective, and adaptable to various materials, surpassing traditional techniques [38–48]. The as-prepared three-dimensional hierarchical solid structures possess uncloneability in surface patterns, holding great promise for anti-counterfeiting applications and boasting encryption capabilities due to their high complexity and diversity. Further efforts can be made to develop more complex and functional diverse hierarchical structures by expanding the types of materials and patterns and, on this basis, broadening their applications.

Supplementary data to this article can be found online at <https://doi.org/10.1016/j.jcis.2025.138202>.

CRediT authorship contribution statement

Wenchang Zhao: Writing – original draft, Visualization, Validation, Methodology, Investigation, Formal analysis, Data curation, Conceptualization. **Shiyu Wang:** Writing – review & editing, Methodology. **Ying Zhou:** Writing – review & editing, Methodology. **Min Wang:** Writing – review & editing, Methodology. **Ling Yang:** Writing – review & editing, Methodology. **Jun Liu:** Writing – review & editing, Methodology. **Liqiu Wang:** Writing – review & editing, Methodology. **Pingan Zhu:** Writing – review & editing, Visualization, Validation, Supervision, Funding acquisition, Formal analysis, Conceptualization.

Declaration of competing interest

The authors declare that they have no known competing financial interests or personal relationships that could have appeared to influence the work reported in this paper. Pingan Zhu and Wenchang Zhao have patent pending to Pingan Zhu and Wenchang Zhao.

Acknowledgments

Funding: This work was supported by the Research Grants Council of Hong Kong (ECS 21213621, GRF17213823, GRF11212321, and GRF11217922) and City University of Hong Kong (7006097).

Data availability

Data will be made available on request.

References

- [1] E. Pitts, J. Greiller, The flow of thin liquid films between rollers, *J. Fluid Mech.* 11 (1961) 33–50, <https://doi.org/10.1017/S0022112061000846>.
- [2] B. Jha, L. Cueto-Felgueroso, R. Juanes, Fluid mixing from viscous fingering, *Phys. Rev. Lett.* 106 (2011) 194502, <https://doi.org/10.1103/PhysRevLett.106.194502>.
- [3] B.S. Broyles, R.A. Shalliker, D.E. Cherrak, G. Guiochon, Visualization of viscous fingering in chromatographic columns, *J. Chromatogr. A* 822 (1998) 173–187, [https://doi.org/10.1016/S0021-9673\(98\)00568-8](https://doi.org/10.1016/S0021-9673(98)00568-8).
- [4] H.E. Huppert, J.A. Neufeld, The fluid mechanics of carbon dioxide sequestration, *Annu. Rev. Fluid Mech.* 46 (2014) 255–272, <https://doi.org/10.1146/annurev-fluid-011212-140627>.
- [5] X. Cheng, L. Xu, A. Patterson, H.M. Jaeger, S.R. Nagel, Towards the zero-surface-tension limit in granular fingering instability, *Nat. Phys.* 4 (2008) 234–237, <https://doi.org/10.1038/nphys834>.
- [6] P.G. Saffman, G. Taylor, The penetration of a fluid into a porous medium or Hele-Shaw cell containing a more viscous liquid, *Proc. R. Soc. London, Ser. A* 245 (1958) 312–329, <https://doi.org/10.1098/rspa.1958.0085>.
- [7] J. Fernandez, P. Kurowski, L. Limat, P. Petitjeans, Wavelength selection of fingering instability inside Hele–Shaw cells, *Phys. Fluids* 13 (2001) 3120–3125, <https://doi.org/10.1063/1.1410120>.
- [8] S. Hill, Channeling in packed columns, *Chem. Eng. Sci.* 1 (1952) 247–253, [https://doi.org/10.1016/0009-2509\(52\)87017-4](https://doi.org/10.1016/0009-2509(52)87017-4).
- [9] I. Bischofberger, R. Ramachandran, S.R. Nagel, Fingering versus stability in the limit of zero interfacial tension, *Nat. Commun.* 5 (2014) 5265, <https://doi.org/10.1038/ncomms6265>.
- [10] V. Sharma, S. Nand, S. Pramanik, C. Chen, M. Mishra, Control of radial miscible viscous fingering, *J. Fluid Mech.* 884 (2020) A16, <https://doi.org/10.1017/jfm.2019.932>.
- [11] K.J. Mloy, J. Feder, T. Jossang, Viscous fingering fractals in porous media, *Phys. Rev. Lett.* 55 (1985) 2688–2691, <https://doi.org/10.1103/PhysRevLett.55.2688>.
- [12] D. Bensimon, L.P. Kadanoff, S. Liang, B.I. Shraiman, C. Tang, Viscous flows in two dimensions, *Rev. Mod. Phys.* 58 (1986) 977, <https://doi.org/10.1103/RevModPhys.58.977>.
- [13] G.M. Homsy, Viscous fingering in porous media, *Annu. Rev. Fluid Mech.* 19 (1987) 271–311, <https://doi.org/10.1146/annurev.fl.19.010187.001415>.
- [14] K.V. McCloud, J.V. Maher, Experimental perturbations to Saffman–Taylor flow, *Phys. Rep.* 260 (1995) 139–185, [https://doi.org/10.1016/0370-1573\(95\)91133-U](https://doi.org/10.1016/0370-1573(95)91133-U).
- [15] J. Nittmann, G. Daccord, H.E. Stanley, Fractal growth viscous fingers: quantitative characterization of a fluid instability phenomenon, *Nature* 314 (1985) 141–144, <https://doi.org/10.1038/314141a0>.
- [16] Y. Couder, O. Cardoso, D. Dupuy, P. Tavernier, W. Thom, Dendritic growth in the Saffman–Taylor experiment, *Europhys. Lett.* 2 (1986) 437, <https://doi.org/10.1209/0295-5075/2/6/005>.
- [17] G. Zocchi, B.E. Shaw, A. Libchaber, L.P. Kadanoff, Finger narrowing under local perturbations in the Saffman–Taylor problem, *Phys. Rev. A* 36 (1987) 1894, <https://doi.org/10.1103/PhysRevA.36.1894>.
- [18] S.D. Kanhurkar, P.S. Gandhi, A. Bhattacharya, Evolution of mesh-like liquid films in multi-port lifted Hele–Shaw cells, *Chem. Eng. Sci.* 252 (2022) 117499, <https://doi.org/10.1016/j.ces.2022.117499>.
- [19] J. Sznitman, Revisiting airflow and aerosol transport phenomena in the deep lungs with microfluidics, *Chem. Rev.* 122 (2022) 7182–7204, <https://doi.org/10.1021/acs.chemrev.1c00621>.
- [20] S. Kumar, Liquid transfer in printing processes: liquid bridges with moving contact lines, *Annu. Rev. Fluid Mech.* 47 (2015) 67–94, <https://doi.org/10.1146/annurev-fluid-010814-014620>.
- [21] D. Derks, A. Lindner, C. Creton, D. Bonn, Cohesive failure of thin layers of soft model adhesives under tension, *J. Appl. Phys.* 93 (2003) 1557–1566, <https://doi.org/10.1063/1.1533095>.
- [22] C. Chen, C. Huang, H. Gadêlha, J.A. Miranda, Radial viscous fingering in miscible Hele–Shaw flows: a numerical study, *Phys. Rev. E* 78 (2008) 016306, <https://doi.org/10.1103/PhysRevE.78.016306>.
- [23] T.U. Islam, P.S. Gandhi, Spontaneous fabrication of three-dimensional multiscale fractal structures using Hele–Shaw cell, *J. Manuf. Sci. Eng.* 139 (2017) 031007, <https://doi.org/10.1115/1.4034624>.
- [24] S. Zhang, E. Louis, O. Pla, F. Guinea, Linear stability analysis of the Hele–Shaw cell with lifting plates, *Eur. Phys. J. B* 1 (1998) 123–127, <https://doi.org/10.1007/s100510050161>.
- [25] J. Nase, D. Derks, A. Lindner, Dynamic evolution of fingering patterns in a lifted Hele–Shaw cell, *Phys. Fluids* 23 (2011) 123101, <https://doi.org/10.1063/1.3659140>.
- [26] S. Brulin, I.V. Roisman, C. Tropea, Fingering instability of a viscous liquid bridge stretched by an accelerating substrate, *J. Fluid Mech.* 899 (2020) A1, <https://doi.org/10.1017/jfm.2020.422>.
- [27] S. Li, J.S. Lowengrub, J. Fontana, P. Palffy-Muhoray, Control of viscous fingering patterns in a radial Hele–Shaw cell, *Phys. Rev. Lett.* 102 (2009) 174501, <https://doi.org/10.1103/PhysRevLett.102.174501>.
- [28] E.O. Dias, E. Alvarez-Lacalle, M.S. Carvalho, J.A. Miranda, Minimization of viscous fluid fingering: a variational scheme for optimal flow rates, *Phys. Rev. Lett.* 109 (2012) 144502, <https://doi.org/10.1103/PhysRevLett.109.144502>.
- [29] D. Pihler-Puzović, P. Illien, M. Heil, A. Juel, Suppression of complex fingerlike patterns at the interface between air and a viscous fluid by elastic membranes, *Phys. Rev. Lett.* 108 (2012) 074502, <https://doi.org/10.1103/PhysRevLett.108.074502>.
- [30] T.T. Al-Housseini, I.C. Christov, H.A. Stone, Two-phase fluid displacement and interfacial instabilities under elastic membranes, *Phys. Rev. Lett.* 111 (2013) 034502, <https://doi.org/10.1103/PhysRevLett.111.034502>.
- [31] H. Zhao, J. Casademunt, C. Yeung, Perturbing Hele–Shaw flow with a small gap gradient, *Phys. Rev. A* 45 (1992) 2455, <https://doi.org/10.1103/PhysRevA.45.2455>.
- [32] T.T. Al-Housseini, P.A. Tsai, H.A. Stone, Control of interfacial instabilities using flow geometry, *Nat. Phys.* 8 (2012) 747–750, <https://doi.org/10.1038/nphys2396>.
- [33] T.T. Al-Housseini, H.A. Stone, Controlling viscous fingering in tapered Hele–Shaw cells, *Phys. Fluids* 25 (2013) 092102, <https://doi.org/10.1063/1.4819317>.
- [34] Z. Zheng, H. Kim, H.A. Stone, Controlling viscous fingering using time-dependent strategies, *Phys. Rev. Lett.* 115 (2015) 174501, <https://doi.org/10.1103/PhysRevLett.115.174501>.
- [35] M. Trojer, M.L. Szulcowski, R. Juanes, Stabilizing fluid–fluid displacements in porous media through wettability alteration, *Phys. Rev. Appl.* 3 (2015) 054008, <https://doi.org/10.1103/PhysRevApplied.3.054008>.
- [36] H.S. Rabbani, D. Or, Y. Liu, N. Shokri, Suppressing viscous fingering in structured porous media, *Proc. Natl. Acad. Sci. USA* 115 (2018) 4833–4838, <https://doi.org/10.1073/pnas.1800729115>.
- [37] T. Gao, M. Mirzadeh, P. Bai, K.M. Conforti, M.Z. Bazant, Active control of viscous fingering using electric fields, *Nat. Commun.* 10 (2019) 4002, <https://doi.org/10.1038/s41467-019-11939-7>.
- [38] T. Cubaud, T.G. Mason, Interacting viscous instabilities in microfluidic systems, *Soft Matter* 8 (2012) 10573–10582, <https://doi.org/10.1039/C2SM25902H>.
- [39] M.C. Tsai, S. Wei, L. Fang, Y. Chen, Viscous fingering as a rapid 3D patterning technique for engineering cell-laden vascular-like constructs, *Adv. Healthc. Mater.* 11 (2022) 2101392, <https://doi.org/10.1002/adhm.202101392>.
- [40] L.L. Bischel, E.W.K. Young, B.R. Mader, D.J. Beebe, Tubeless microfluidic angiogenesis assay with three-dimensional endothelial-lined microvessels, *Biomaterials* 34 (2013) 1471e1477, <https://doi.org/10.1016/j.biomaterials.2012.11.005>.
- [41] R. Kay, C. Katrycz, K. Nitiema, J.A. Jakubiec, B.D. Hatton, Decapod-inspired pigment modulation for active building facades, *Nat. Commun.* 13 (2022) 4120, <https://doi.org/10.1038/s41467-022-31527-6>.
- [42] S. Jia, T. Tao, J. Sun, J. Du, Y. Xie, L. Yu, W. Tang, J. Wang, J. Gong, Understanding hierarchical structure construction strategies and biomimetic design principles: a review, *Small Struct.* 4 (2023) 2300139, <https://doi.org/10.1002/ssr.202300139>.
- [43] S.S. Deshmukh, A. Goswami, Recent developments in hot embossing—a review, *Mater. Manuf. Process.* 36 (2021) 501–543, <https://doi.org/10.1080/10426914.2020.1832691>.
- [44] J.L. Charest, L.E. Bryant, A.J. Garcia, W.P. King, Hot embossing for micropatterned cell substrates, *Biomaterials* 25 (2004) 4767–4775, <https://doi.org/10.1016/j.biomaterials.2003.12.011>.
- [45] T. Ding, Q. Zhao, S.K. Smoukov, J.J. Baumberg, Selectively patterning polymer opal films via microimprint lithography, *Adv. Opt. Mater.* 2 (2014) 1098–1104, <https://doi.org/10.1002/adom.201400327>.
- [46] S. Kang, Y.J. Park, J.Y. Hwang, H.J. Jeong, J.S. Lee, K.J. Kim, H.-C. Kim, J. Huh, C. Park, Localized pressure-induced ferroelectric pattern arrays of semicrystalline poly(vinylidene fluoride) by microimprinting, *Adv. Mater.* 19 (2007) 581–586, <https://doi.org/10.1002/adma.200601474>.
- [47] W. Zhao, Y. Yan, X. Chen, T. Wang, Combining printing and nanoparticle assembly: methodology and application of nanoparticle patterning, *Innovation* 3 (2022) 100253, <https://doi.org/10.1016/j.xinn.2022.100253>.
- [48] D. Qin, Y. Xia, G.M. Whitesides, Soft lithography for micro- and nanoscale patterning, *Nat. Protoc.* 5 (2010) 491–502, <https://doi.org/10.1038/nprot.2009.234>.
- [49] W.R. Childs, R.G. Nuzzo, Decal transfer microlithography: a new soft-lithographic patterning method, *J. Am. Chem. Soc.* 124 (2002) 13583–13596, <https://doi.org/10.1021/ja020942z>.
- [50] W. Lieu, D. Fang, K.J. Tay, X. Li, W. Chu, Y.S. Ang, D. Li, L.-K. Ang, Y. Wang, H. Yang, Progress on 3D-printed metal-organic frameworks with hierarchical structures, *Adv. Mater. Technol.* 7 (2022) 2200023, <https://doi.org/10.1002/admt.202200023>.
- [51] C. Zhu, H.B. Gameda, E.B. Duoss, C.M. Spadaccini, Toward multiscale, multimaterial 3D printing, *Adv. Mater.* 36 (2024) 2314204, <https://doi.org/10.1002/adma.202314204>.
- [52] O. Lyutakov, J. Tüma, I. Huttel, V. Prajzler, J. Siegel, V. Švorčík, Polymer surface patterning by laser scanning, *Appl. Phys. B Lasers Opt.* 110 (2013) 539–549, <https://doi.org/10.1007/s00340-012-5291-3>.
- [53] M.S. Hahn, J.S. Miller, J.L. West, Laser scanning lithography for surface micropatterning on hydrogels, *Adv. Mater.* 17 (2005) 2939–2942, <https://doi.org/10.1002/adma.200500184>.

- [54] S. Liang, Random-walk simulations of flow in Hele Shaw cells, *Phys. Rev. A* 33 (1986) 2663, <https://doi.org/10.1103/PhysRevA.33.2663>.
- [55] P. Meakin, Diffusion-controlled cluster formation in 2–6-dimensional space, *Phys. Rev. A* 27 (1983) 1495–1507, <https://doi.org/10.1103/PhysRevA.27.1495>.
- [56] R. Lenormand, C. Zarcone, Invasion percolation in an etched network: measurement of a fractal dimension, *Phys. Rev. Lett.* 54 (1985) 2226, <https://doi.org/10.1103/PhysRevLett.2226>.